Chemical Engineering Science 247 (2022) 116925

Contents lists available at ScienceDirect

Chemical Engineering Science

journal homepage: www.elsevier.com/locate/ces

Non-linear boundary conditions for the convection-diffusion equation in lattice Boltzmann framework

Elham Kashani [a], Ali Mohebbi [a,*], Amir Ehsan Feili Monfared [b], Amir Raoof [c]

[a] Department of Chemical Engineering, Faculty of Engineering, Shahid Bahonar University of Kerman, Kerman, Iran
[b] Department of Chemical Engineering, Graduate University of Advanced Technology, Kerman, Iran
[c] Environmental Hydrogeology, Department of Earth Sciences, Utrecht University, Utrecht, the Netherlands

HIGHLIGHTS

- A method for the implementation of Robin boundary condition in 2D LBM is introduced.
- The method suggests using a coupling of Taylor expansion and counter-slip approach.
- The method can impose nonlinear reaction kinetics in lattice Boltzmann framework.
- The method can impose surface radiation condition in lattice Boltzmann framework.
- Order of convergence rate is a function of the nonlinearity of the condition.

GRAPHICAL ABSTRACT

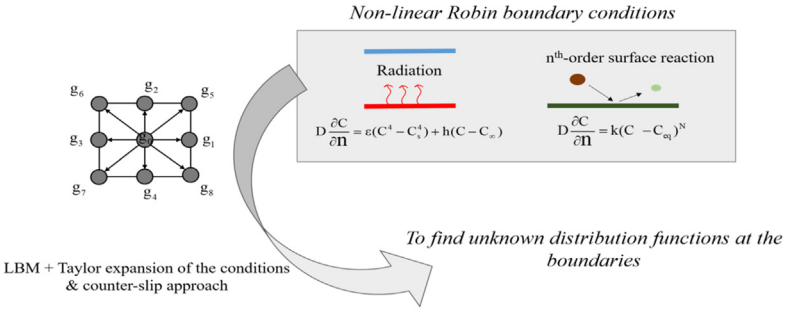

ARTICLE INFO

Article history:
Received 24 March 2021
Received in revised form 24 June 2021
Accepted 4 July 2021
Available online 6 July 2021

Keywords:
Lattice Boltzmann method
Convection-diffusion
Non-linear Robin boundary condition
Radiation
N^{th}-order surface reaction
Fracture

ABSTRACT

Implementation of nonlinear boundary conditions like n^{th}-order surface reactions or surface radiation heat transfer has not been investigated in lattice Boltzmann (LB) framework. This study presents a novel kinetic level method for their implementation. The method couples Taylor expansion of the conditions with counter-slip approach to find unknown distribution functions at boundary nodes. The proposed scheme guarantees the locality and orientation independency of formulations. To evaluate the proposed scheme performance, several 1D and 2D test cases were simulated by D2Q9 LBM and the outcomes were compared with analytical and numerical solutions. The geometry evolution by n^{th}-order surface reaction was investigated for dissolutions in a simple fracture and a spherical carbonate particle in a channel. The results demonstrated the method performs promisingly in terms of accuracy. The convergence rate of scheme based on the results from l^2-norm analyses showed first or second-order rates of convergence, depending on constraint's degree of nonlinearity.

1. Introduction

Lattice Boltzmann equation (LBE) has been applied to simulate complicated heat, mass, and momentum transfer problems like multiphase, multicomponent, and reactive flows (He and Doolen, 2002; Mohamad, 2011; Ponce Dawson et al., 1993; Shan and Doolen, 1995; Tian et al., 2014). Some advantages of LBE that make

* Corresponding author.
E-mail addresses: amohebbi@uk.ac.ir, amohebbi2002@yahoo.com (A. Mohebbi), e.monfared@kgut.ac.ir (A.E. Feili Monfared), a.raoof@uu.nl (A. Raoof).

https://doi.org/10.1016/j.ces.2021.116925
0009-2509/

it popular for simulations are the simplicity of programming and the parallel nature of the algorithms. However, despite these promising features, applying boundary conditions in the lattice Boltzmann method (LBM) is not a straightforward task and overcoming the corresponding challenges has been the subject of many studies in the past two decades. Implementing boundary conditions in LBM is intrinsically different from the traditional macroscopic computational fluid dynamics (CFD) methods. The conventional CFD methods are based on numerical discretizing of macroscopic equations, while LBM employs the classical kinetic theory and the statistical distribution functions as its computation basis. In LBM, fractious particles replace the fluid and the distribution functions represent the properties of particles.

To implement boundary conditions in this framework, the unknown entering distribution functions at the boundary nodes should be correctly calculated. Especially for the scalar transport governed by the convection-diffusion equation, various studies have been performed on implementation methods of Dirichlet and Neumann boundary conditions. One of the first boundary conditions presented for the convection-diffusion equation was the one introduced by He et al. (He et al., 1998). They employed the bounce-back of nonequilibrium idea proposed by Zou and He (Zou and He, 1997) to generalize the previously proposed hydrodynamic boundary condition to heat transfer cases. In another work, Ginsberg (Ginzburg, 2005) presented a multi-reflection approach for the imposition of Dirichlet and Neumann boundary conditions. Tang et al. (Tang et al., 2005) proposed the idea of decomposing the unknown distribution populations into equilibrium and nonequilibrium parts. The nonequilibrium part was approximated with an extrapolation of the neighboring populations. In 2013, Chen et al. (2013) proposed an improved bounce-back method by using the midpoint concentration value. Huang et al. (2011) proposed an extrapolation scheme for Dirichlet and Neumann boundary conditions following the idea of the regularized scheme of Latt et al. (2008). They also compared different boundary implementation schemes including the regularized method, simple extrapolation, non-equilibrium extrapolation, simple bounce-back, and equilibrium schemes. The works on the first type and second type boundary conditions have not been restricted to straight boundaries (Ginzburg, 2005; Latt et al., 2008; Li et al., 2013) and several boundary methods have been proposed for the treatment of the curved ones; however, it should be noted that their implementations -especially in complex media- are rather difficult. Moving boundaries have also been the focus of some researches. Mozafari-shamsi et al. (2018) simulated the heat transfer from moving bodies with curved boundaries by combining ghost-fluid LBM (GF-LBM) and a refiling scheme. According to their results, the GF-LBM with refilling could simulate the thermal moving curved boundaries with high accuracy.

Implementation of the linear Robin boundary conditions for the convection-diffusion equation has also been the subject of many studies. He et al. (He et al., 2000) presented a lattice Boltzmann scheme to simulate the convection-diffusion problem with surface chemical reactions. In 2002, Kang et al. (2002b) employed a modification of the nonequilibrium scheme and proposed a Robin boundary for simulating dissolution of porous media. Their underlying approach was based on the observation that the nonequilibrium portion of the distribution functions is proportional to the dot product of their microscopic velocity and the concentration gradient. In another work, Walsh and Saar (2010) proposed an interpolation boundary condition to simulate first-order reaction kinetics. Zhang et al. (2012) presented a bounce-back scheme to implement general thermal/concentration boundary conditions, including either Dirichlet, Neumann, or Robin boundary conditions. However, their scheme suffered from first-order accuracy mainly because a first-order finite difference scheme was adopted for the normal derivative. With an asymptotic analysis technique, Huang and Yong (2015) suggested two boundary schemes for the general Robin boundary condition. Although their second scheme -in contrast to the first one- could also account for curved boundaries, but it only offered first-order accuracy. Recently, a reactive boundary scheme for irregular geometries with linear heterogeneous surface reaction is presented by Ju et al. (2020). Their scheme can easily be applied to problems with complex geometries.

Despite the rich literature introducing the methods of implementing the more common conditions, i.e., Dirichlet, Neumann, and linear Robin boundary conditions, the non-linear Robin conditions are rarely found in the literature. In fact, most dissolution-precipitation cases studied in the LBM framework are essentially restricted to first-order reaction kinetics, or similarly for the energy transport, they are mainly limited to Newton's law of cooling which is a linear constraint. This is while the nonlinear constraints (for example the surface radiation case) which are of great practical importance to industry, have been rarely considered in the literature. One of the few examples is the work of Kang et al. (Kang et al., 2006) on multicomponent reactive transport in porous media. In this study, the Newton-Raphson method was used to impose a nonlinear algebraic constraint and to calculate the concentration of the species at boundary nodes. In more recent work, Huber et al. (2014) employed a phase-field method and presented a new pore-scale model for non-linear heterogeneous reactions. In their model, the surface reaction was not explicitly imposed as a boundary condition and alternately was treated as a source or sink term in the governing transport equations. Accordingly, solid-fluid boundary nodes were considered as part of the solution domain and therefore the algorithm was independent of the surface shapes and grains' orientation. In 2016, the Counter-slip energy approach was employed by Monfared et al. (Feili Monfared et al., 2016) to derive kinetic level nonlinear boundary constraints. These constraints represented convection and also a combination of convection and surface radiation at boundary nodes, which – from a mathematical point of view – are regarded as linear and nonlinear Robin boundary conditions, respectively. However, their research was only restricted to fourth-degree nonlinear Robin boundary conditions which is mainly encountered in surface radiation simulations.

It should be pointed out here that except for the mentioned studies, the treatment of nonlinear Robin boundary conditions in LBM framework has been rarely investigated in the literature and to the best knowledge of the authors no general scheme capable of imposing nonlinear constraints with any arbitrary exponent (degree) is proposed so far. However, these types of constraints are of wide engineering applications especially for the field of reactive transport in geochemical systems, where many mineral reactions have nonlinear kinetics. Accordingly, in this research, proposal of a general method for the implementation of nonlinear Robin boundary conditions with any arbitrary degree is intended. Hence, the remainder of this paper is organized as follows. In Section 2 lattice Boltzmann method and the corresponding equations are explained. In Section 3 a novel method for imposing nonlinear Robin constraints is proposed and in Sections 3.1 and 3.2, the scheme is discussed for two special cases, i.e., surface radiation boundary condition and nth-order heterogeneous reaction kinetics, respectively. Finally, in Section 4 the performance and accuracy of the method is evaluated with several 1D and 2D test cases.

2. Lattice Boltzmann method

In this section, a brief introduction about LBM and the governing equations is given. Convection-diffusion equation (CDE) that

describes the transport of a passive scalar which could be energy in heat transfer or mass in the mass transfer is considered as follows (Huang et al., 2011)

$$\frac{\partial C}{\partial t} + \nabla \cdot (uC) = \nabla \cdot (D \nabla C) \tag{1}$$

in which C is a scalar quantity, D is the diffusion coefficient, and $u$is the velocity vector. It can be shown that the CDE equation (Eq. (1)) can be derived from the LBE through a Chapman-Enskog expansion procedure (Chai and Zhao, 2013). In this study, among different LBE collision models, the Bhatnagar-Gross-Krook model (BGK) was employed mainly because of its simplicity and high computational efficiency (Huang et al., 2011)

$$g_i(x + c_i\Delta t, t + \Delta t) - g_i(x,t) = \frac{1}{\tau}\left[g_i^{eq}(C,u) - g_i(x,t)\right] \quad \begin{cases} X = x, y \\ i = 0, \ldots, 8 \\ u = u_x, u_y \end{cases} \tag{2}$$

where $g_i(\mathbf{X},t)$ is the particle distribution function along i direction with C_i being discrete velocity. In this work, the more popular D2Q9 scheme representing nine discrete particle velocity in a 2D domain was used. C_i is specified to be one i.e. $c_i \equiv \frac{\Delta x}{\Delta t} = 1$, while Δx and Δt are the linkage length and time step.$\tau$is the relaxation time related to the diffusion coefficient by $D = c_s^2(\tau - 0.5)$and c_s is the speed of sound, c_s = 1/3. In Eq. (2), $g_i^{eq}$is the equilibrium distribution function calculated from Eq. (3) (Kang et al., 2003):

$$g_i^{eq}(C,u) = w_i C\left[1 + \frac{3c_i.u}{c^2} + \frac{9(c_i.u)^2}{2c^4} - \frac{3u.u}{2c^2}\right] \tag{3}$$

The hydrodynamic field is also found by solving the lattice Boltzmann transport equation of the form Eq. (4) (Kang et al., 2003):

$$f_i(x + c_i\Delta t, t + \Delta t) - f_i(x,t) = \frac{1}{\tau'}\left[f_i^{eq}(\rho,u) - f_i(x,t)\right] \tag{4}$$

where f_i is the particle distribution function,τ' is the relaxation time that is related to the kinematic viscosity by $v = c_s^2(\tau' - 0.5)$, and f_i^{eq} is the equilibrium distribution function that has the following form for D2Q9 model (Kang et al., 2003).

$$f_i^{eq}(C,u) = w_i\rho\left[1 + \frac{3c_i.u}{c^2} + \frac{9(c_i.u)^2}{2c^4} - \frac{3u.u}{2c^2}\right] \tag{5}$$

here$\rho$is the fluid density, and w_i is the corresponding weight coefficients. Discrete velocities and weight coefficients for D2Q9 model are defined as (Kang et al., 2003):

$$\begin{cases} c_i = (0,0) \;\; ; \;\; w_i = \frac{4}{9} & i = 0 \\ c_i = \left(\cos\frac{(i-1)\pi}{2}, \sin\frac{(i-1)\pi}{2}\right) \;\; ; \;\; w_i = \frac{1}{9} & i = 1-4 \\ c_i = \sqrt{2}\left(\cos\left[\frac{(i-5)\pi}{2} + \frac{\pi}{4}\right], \sin\left[\frac{(i-5)\pi}{2} + \frac{\pi}{4}\right]\right) \;\; ; \;\; w_i = \frac{1}{36} & i = 5-8 \end{cases} \tag{6}$$

By using the Chapman-Enskog expansion, it can be proved that the continuity and momentum equations for macroscopic scale are recovered (Guo and Zhao, 2002). The macroscopic scalar quantities, velocity, and density are calculated by the following equations (Kang et al., 2003):

$$C = \sum_{i=0}^{8} g_i \tag{7}$$

$$\rho = \sum_{i=0}^{8} f_i \tag{8}$$

$$u_\alpha = \sum_{i=0}^{8} c_{i\alpha} f_i \quad \alpha = x, y \tag{9}$$

3. Methodology

The method proposed in this study generally consists of a linearization step followed by a closure construction step for the system of equations. To perform the linearization, Taylor expansion of the nonlinear boundary constraint was employed and for the purpose of system closure, the equilibrium idea of Inamuro et al. (Inamuro et al., 1995) was adopted. It is worth noting that it is not the first time that the idea of Inamuro et al. (Inamuro et al., 1995) is being used for the boundary conditions of the convection-diffusion equation in LBM framework and the core idea has been previously used in several studies (D'Orazio et al., 2004; D'Orazio and Succi, 2003; Karimipour, 2012).

To evaluate this method, a number of scenarios related to heat and mass transfer problems were simulated and analyzed. The general framework of this section is depicted in Fig. 1. For heat transfer problems, a boundary condition for the combination of surface radiation and convection was developed and the results were compared with a previous study. Also, for mass transfer applications, a general non-linear Robin boundary condition for n^{th}-order surface reactions was formulated. It is worth noting that the method is such designed that could be easily applied to complex geometries such as those usually seen in naturally occurring porous media.

3.1. Combined radiation and convection boundary condition

To discuss a sample nonlinear boundary condition in heat transfer systems, a combination of surface radiation and convection at a boundary is considered here. The mathematical formulation for this type of constraint is given in Eq. (10) (Feili Monfared et al., 2016):

$$D\frac{\partial C}{\partial y} = \varepsilon(C^4 - C_s^4) + h(C - C_\infty) \tag{10}$$

where C represents temperature at boundary node. The first and the second terms on the right-hand side represent radiation and

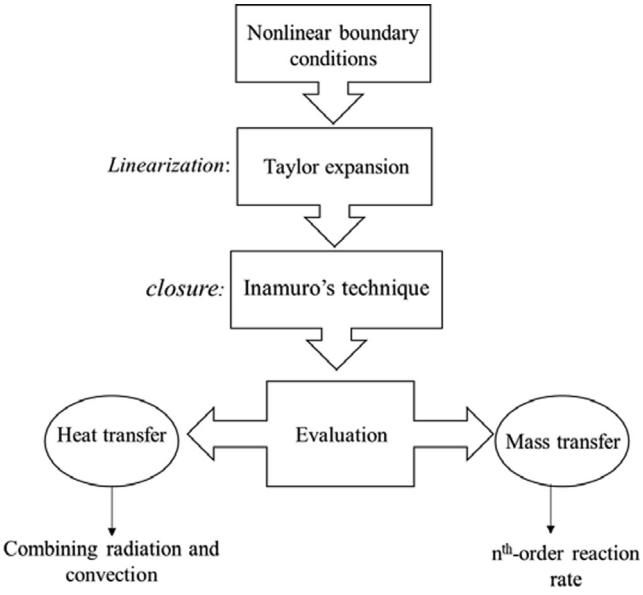

Fig. 1. General framework of methodology section.

convection, respectively. Implementing such a boundary condition in the LBM framework was first studied by Monfared et al. (Feili Monfared et al., 2016). They employed the counter-slip approach and solved the resulting quartic equations with a tedious algorithm. Assuming this boundary condition to be imposed on a bottom wall, the term on the left-hand side of this equation would represent the heat flux along the y-direction.

In general, the total flux along the normal direction of the surface at the boundary nodes can be expressed as (Ju et al., 2020):

$$total\ flux\ along\ n: \sum_i n.c_i g_i = j_d + j_w \tag{11}$$

where j_d and j_w represent the fluxes due to molecular diffusion and the wall motion, respectively. Thus, assuming stationary walls, it can be shown that (Ju et al., 2020):

$$j_d \approx -c_s^2 \tau \Delta t \frac{\partial C}{\partial n} = -\gamma D \frac{\partial C}{\partial n} \tag{12}$$

where $\gamma = \frac{\tau}{\tau - 0.5}$. By combining Eqs. (11) and (12), Eq. (13) is achieved:

$$\sum_i n.c_i g_i = -\gamma D \frac{\partial C}{\partial n} \tag{13}$$

Considering the velocity naming convention presented in Fig. 2 and assuming the condition to be imposed on the bottom wall, combination of Eqs. (10) and (13) gives:

$$(g_5 + g_2 + g_6) - (g_7 + g_4 + g_8) = -\gamma(\varepsilon(C^4 - C_s^4) + h(C - C_\infty)) \tag{14}$$

To linearize Eq. (14), first-order Taylor expansion of C^4 around $\hat{C}$ was employed:

$$C^4 \cong \hat{C}^4 + 4\hat{C}^3(C - \hat{C}) \tag{15}$$

where $\hat{C}$ is the scalar quantity (temperature) at the boundary node in a previous iteration. Hence, combining Eqs. (14) and (15) gives:

$$(g_5 + g_2 + g_6) - (g_7 + g_4 + g_8) = -\gamma(\varepsilon(\hat{C}^4 + 4\hat{C}^3(C - \hat{C}) - C_s^4) + h(C - C_\infty)) \tag{16}$$

The unknown distribution functions on the bottom wall are $g_2, g_5,$ *and* g_6 for which Eq. (16) should be solved. To overcome the challenge of underdetermination of the system of equations and close the problem, Inamuro's idea for boundary conditions (Inamuro et al., 1995; Yoshino and Inamuro, 2003) was employed. Inamuro et al. assumed the unknown distribution functions to be equal to their equilibrium condition at a new unknown condition, C':

$$g_i = g_i^{eq}(C', u) \tag{17}$$

By substituting Eqs. (3), 7, and 17 into Eq. (16) and letting u = 0, C' is found:

$$C' = 6 \times \frac{(g_7+g_4+g_8)(1-4\gamma\varepsilon\hat{C}^3-\gamma h)-(g_0+g_1+g_3)(4\gamma\varepsilon\hat{C}^3+\gamma h)+\gamma\varepsilon(3\hat{C}^4+C_s^4)+\gamma h C_\infty}{1+4\gamma\varepsilon\hat{C}^3+\gamma h} \tag{18}$$

Having calculated C' by Eq. (18), the unknown populations can be calculated by Eq. (17).

3.2. Nonlinear heterogeneous reaction kinetics

In most numerical LBM studies, to explore dissolution-precipitation processes, first-order reaction kinetics are commonly assumed(Kalia and Glasbergen, 2009; Ma et al., 2017; Molins et al., 2020; Mostaghimi et al., 2016). However, in more realistic systems such as those commonly encountered in hydrogeochemical processes (Lasaga, 2014), nonlinear reaction kinetics would be of more essential importance for a successful description of the underlying phenomena. Despite this major concern, and to the best knowledge of the authors, no LBM study regarding non-linear reaction kinetics is published so far. Accordingly, proposal of a general n^{th}-order reaction boundary condition in LBM framework is intended in this section. A general form of such surface reactions is shown in Eq. (19). Those interested in these reactions and further discussions are referred to (Jeschke and Dreybrodt, 2002; Lasaga, 2014) as some examples.

$$D\frac{\partial C}{\partial n} = k(C - C_{eq})^N \tag{19}$$

This empirical rate equation is commonly seen in many natural processes such as dissolution of limestones (Ague, n.d.; Jeschke and Dreybrodt, 2002; Yi et al., 2014). The term on the left-hand side represents the flux along the normal direction and the right-hand side term indicates dissolution rate which depends on the undersaturation condition (Keir, 1980). In this equation C stands for concentration, C_{eq} is an equilibrium or saturation concentration, N is the order of reaction, $\mathbf{n}$ is the unit normal vector at the boundary, and k is the reaction rate coefficient. Combining Eqs. (13) and (19), Eq. (20) is obtained.

$$\sum_i n.c_i g_i = -\gamma k(C - C_{eq})^N \tag{20}$$

Using Taylor expansion similar to that of the previous section and following the linearization procedure for $S \cong (C - C_{eq})^N$ gives:

$$S \cong \hat{S} + (\frac{d\hat{S}}{dC})(C - \hat{C}) \tag{21}$$

For more convenience, the links at a boundary node are divided into two groups of A_s (representing the unknown directions) and A_f (representing the remaining known links). Hence, Eq. (20) can be rewritten as:

$$\sum_{i\in A_s} n.c_i g_i + \sum_{i\in A_f} n.c_i g_i = -\gamma k\left[\left(\hat{C} - C_{eq}\right)^N + N\left(\hat{C} - C_{eq}\right)^{N-1}(C - \hat{C})\right] \tag{22}$$

Since $C = \sum_{i\in A_s} g_i + \sum_{i\in A_f} g_i$ and by substituting Eq. (17) into Eq. (22) for the unknown distributions (A_s), the following equation is derived:

$$C' = \frac{-\sum_{i\in A_f} n.c_i g_i - \gamma k(\hat{C} - C_{eq})^{N-1}\left[(\hat{C} - C_{eq}) - N(\hat{C} - \sum_{i\in A_f} g_i)\right]}{\sum_{i\in A_s} w_i n.c_i + \gamma k N(\hat{C} - C_{eq})^{N-1}\sum_{i\in A_s} w_i} \tag{23}$$

From dot product definition, $n.c_i = |n||c_i|\cos\alpha$, n *and* α are interface normal vector and the angle between the normal vector and velocity link, respectively. n *and* α could be obtained from methods like volume of fluid (Pilliod and Puckett, 2004; Rudman, 1997; Youngs, 1984) or they could be approximated by the lattice link direction (Kang et al., 2006, 2002; Zhang et al., 2012). Having found C' the unknown populations can be easily calculated from Eq. (17).

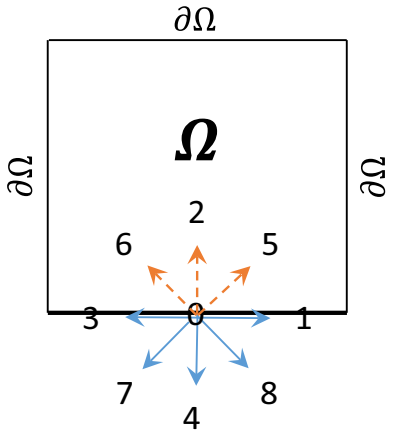

Fig. 2. Discretized velocities for a D2Q9 model with dashed arrows representing unknown directions on the bottom wall.

4. Results and discussion

4.1. Combining surface radiation and convection

To investigate the performance of the proposed boundary scheme, the problem of conduction in a square slab is considered here. The vertical walls are assumed adiabatic, constant temperature condition is defined for the upper wall and the bottom wall is subjected to combined convection and surface radiation. Schematic of the geometry and the corresponding imposed constraints are shown in Fig. 3.

By setting zero flux on lateral vertical boundaries, the mathematical formulation reduces to a conceptually 1D problem with available analytical solutions. The general solution would be of the form $C = a_1 y + a_2$ in which a_1 *and* a_2 are constant values:

$$a_1 = \frac{C_{up} - a_2}{L} \tag{24}$$

and a_2 is the root of Eq. (25):

$$L\varepsilon a_2^4 + (D + hL)a_2 - L\varepsilon C_s^4 - hLC_\infty - DC_{up} = 0 \tag{25}$$

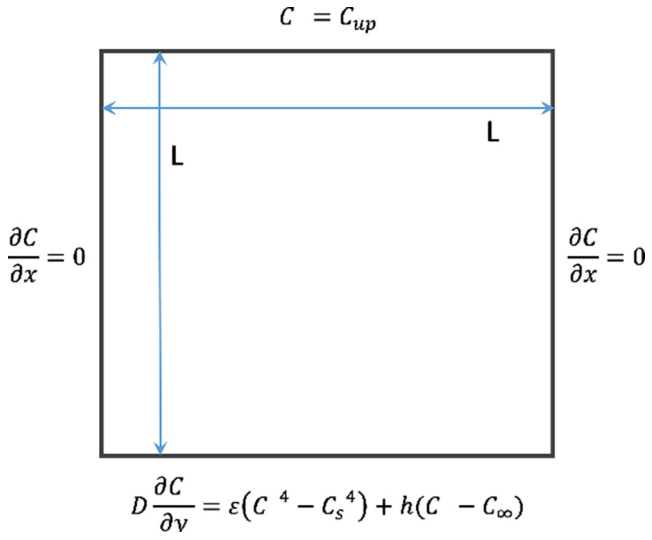

Fig. 3. Geometry of diffusion in a slab with combined convection and surface radiation from the bottom.

In simulations, L, C_s, C_∞, C_{up}, and Dwere assumed to be 100, 0.0, 5.0 10.0 and 0.22, respectively (Feili Monfared et al., 2016). A comparison of the simulation results with the analytical solutions is used for method performance analysis. Results from a previous study (Feili Monfared et al., 2016) are also presented for comparison purposes. Fig. 4 (a) shows temperature variation in vertical center-line (i.e., $C(50, y)$) for different (ε, h)values. It is clear from the figure that the numerical results of the presented method match very well with the results of Monfared et al. and analytical solutions. It should be pointed out here that although the method presented by Monfared et al. calculates the exact root of the governing boundary equations and therefore is expected to be more accurate, but the method proposed in this study -in contrast to (Feili Monfared et al., 2016)- is not restricted to quartic constraints and can be applied for any boundary constraint of arbitrary degree with acceptable accuracy. This feature is crucially important especially for mineral reaction boundary conditions where non-integer exponents are very common. Additionally, to better see the one-dimensionality of the temperature profile, the contour of temperature for special case of $(\varepsilon, h) = (0.1, 1)$is depicted in Fig. 4 (b).

Furthermore, to estimate the global error, relative l^2-norm of the domain (Er) was adopted (Feili Monfared et al., 2016).

$$E_r = \frac{\| C - C_{exact} \|}{\| C_{exact} \|} = \left(\frac{\sum_{all\ nodes} (C - C_{exact})^2}{\sum_{all\ nodes} (C_{exact})^2} \right)^{0.5} \tag{26}$$

where C and C_{exact} represent the numerical and analytical scalar variables, respectively. Table 1 provides the relative l^2-norm (Er) of the domain for different values of ε and h. As can be deduced from Fig. 4(a) and Table. 1, there is only marginal errors between the analytical solutions and the numerical results; demonstrating the effectiveness of the method.

To check the convergence rate of the method, the relative l^2-norm of the domain versus the reciprocal of mesh size is plotted for different relaxation times in Fig. 5. As shown in this figure, the trend of increasing Er by decreasing the grid resolution for all$\tau$is almost linear with a slope of more than unity. It reveals a first-order convergence of the presented method for the combination of convection and surface radiation.

4.2. N^{th}-order reaction rate

In the next two following subsections, the accuracy of the presented formulation (Eq. (23)) is evaluated in 1D and 2D simulations. For the 1D case, analytical solutions of the problem were available and were preferably used for validation purposes. However, for 2D problems, no analytical solutions were available. Accordingly, the corresponding macroscopic equation (Eq. (1)) was solved by the finite volume method (FVM) and the results were compared with those of LBM.

It should also be emphasized that the proposed scheme is fully local and orientation-independent (see Section 4.2.3 for more explanation). Since these features make this method a good candidate for employment in complex geometries, its performance in such cases is also of interest. Accordingly, the last part of this section is devoted to the problem of reactive flow in a simple fracture. The method is used to simulate the time evolution of the geometry by the imposed nonlinear reaction kinetics and the results are compared with analytical solutions.

4.2.1. 1D simulation

In this section, a geometry almost similar to that of Fig. 3 is considered. The only difference is that the bottom wall boundary condition is replaced by Eq. (23). As explained before, the analyti-

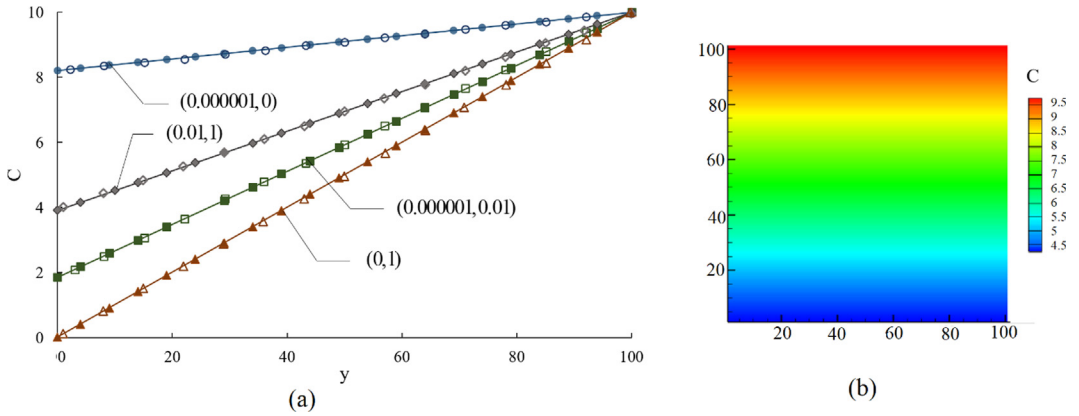

Fig. 4. **(a)** Temperature variation in vertical centerline for different values of (ε, h); Lines, filled, and non-filled markers indicate analytical and numerical results of the presented method and Monfared et al. (Feili Monfared et al., 2016) study, respectively. **(b)** contours of temperature (C) for.$(\varepsilon, h) = (0.01, 1)$.

Table 1
Relative l^2-norm (Er) for different values of.(ε, h).

(ε, h)	(0.000001,0)	(0.000001,0.01)	(0.01,1)	(0,1)
Er	0.00072	0.0009	0.00017	0.00014

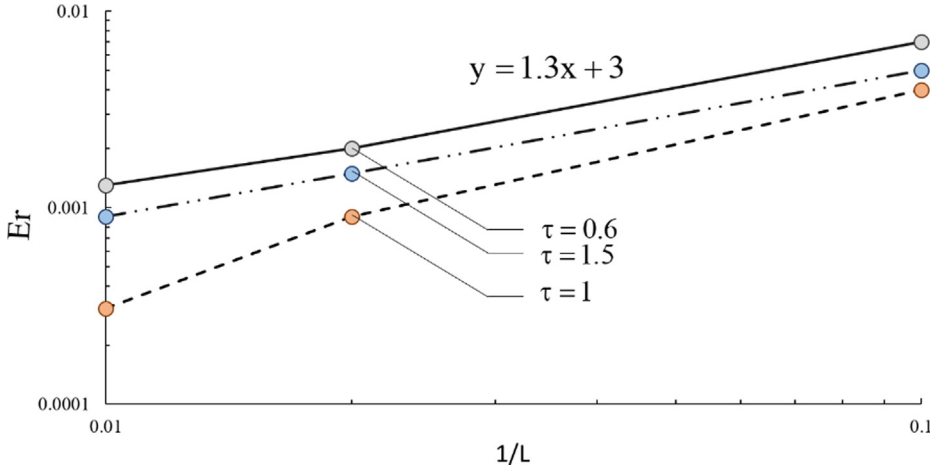

Fig. 5. Relative l^2-norm of the domain (Er) as a function of relaxation time and grid resolution (1/L).

cal solution would be of the form $C = a_1 y + a_2$, where a_1 is calculated by Eq. 24 and a_2 is the root of Eq. (27):

$$kL(a_2 - C_{eq})^N + Da_2 - DC_{up} = 0 \tag{27}$$

To find the roots of Eq. (27), the Newton method was applied. Simulations for 3 different pairs of (N,C_{eq}) were conducted and the numerical and analytical results are shown in Fig. 6. In these simulations C_{up}, k, and D were fixed at 10.0, 0.06, and 0.22, respectively.

Results of Fig. 6 demonstrate that both LBM and FVM simulations have very well approximated the analytical solutions. Furthermore, relative l^2-norms of the domain for different reaction orders (N) and different relaxation times (τ)are illustrated in Fig. 7. Considering the figure reveals that the presented method offers acceptable accuracy for a wide range of relaxation times and *N* values. However, it should be pointed out that accuracy of LBM is generally a function of relaxation time and as can be seen, at low relaxation times, the error of the proposed method did not change with the order of reaction but at higher relaxation times, by increasing *N* the error is decreased.

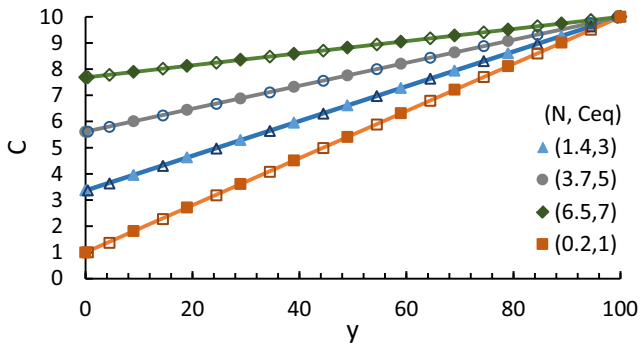

Fig. 6. 1D concentration variation in y-direction at different values of (N, Ceq). Lines, filled and non-filled markers indicate analytical, LBM and FVM results, respectively.

The convergence rate of the method for a special case of N = 0.5 was also investigated. Fig. 8 shows the results of the relative l^2-norm of the domain versus the reciprocal of the mesh size. As

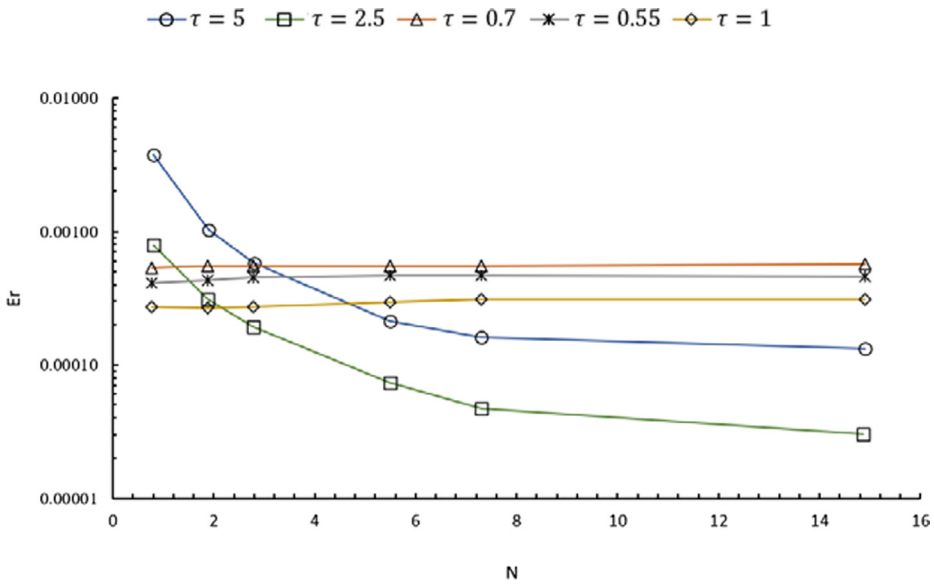

Fig. 7. Relative l^2-norm (Er) of LBM at different relaxation times versus exponent N.

can be observed, the method offers a convergence rate of about 2 for different values of relaxation time.

4.2.2. 2D diffusion

To further analyze the performance of the proposed method, 2D simulations of the diffusion process in the square domain of Fig. 9 were also investigated.

The boundary condition at the lower wall represents a chemical reaction (Eq. (19)) whereas constant concentration, C_w, at the left and right walls is imposed. In addition, the upper wall is assumed to be impermeable (i.e., no flux condition). The governing equations of the macroscopic process are given in Appendix A.

To analyze the performance of the method, LBM and FVM simulations of the problem for serval values of N and C_w were performed. Other simulation parameters were defined as k = 0.06, C_{eq} = 1.0 and τ = 1.0. It is worth mentioning that the relaxation time is not explicitly incorporated in the FVM method and its value should be mapped into its macroscopic counterpart which is the diffusion coefficient for the present case. Regarding Fig. 10, the horizontal and vertical center-line concentration profiles are depicted for 3 different pairs of (N, C_w). Clearly, the proposed method has performed very well over the range of tested exponents and the LBM results show conformity with those of FVM.

4.2.3. Transport in reactive flow

To evaluate the performance of the proposed scheme for more complex conditions, the acid-carbonate reaction was simulated (Fig. 11) and the results were compared with those of Molins et al. (2020). As shown in Fig. 11, the acid enters a rectangular domain with a uniform inlet velocity and constant inlet concentration C, and after reacting with the spherical carbonate grain ($CaCO_3$) exits at a predetermined pressure. In Molins et al. (2020), the reaction on the interface of the grain was assumed to

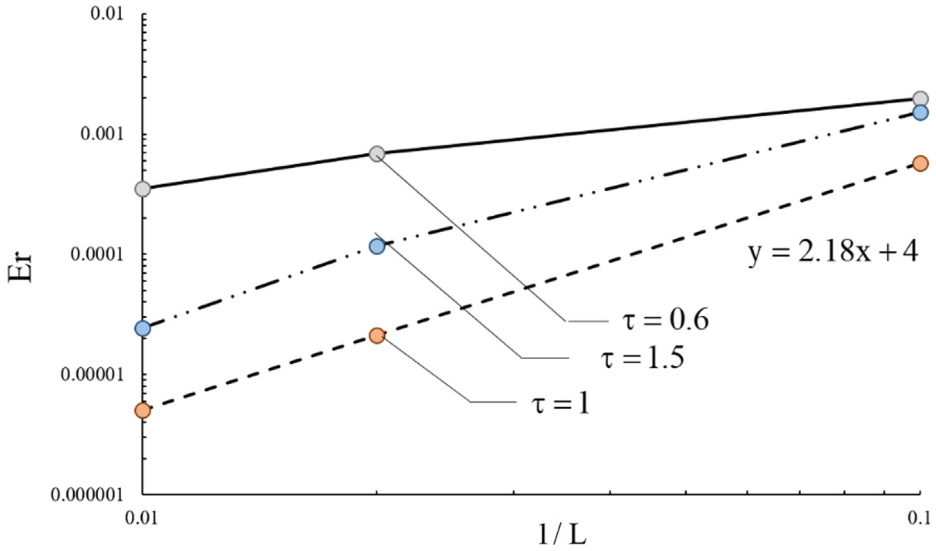

Fig. 8. Relative l^2-norm of the domain (Er) as a function of relaxation time and grid resolution (1/L).

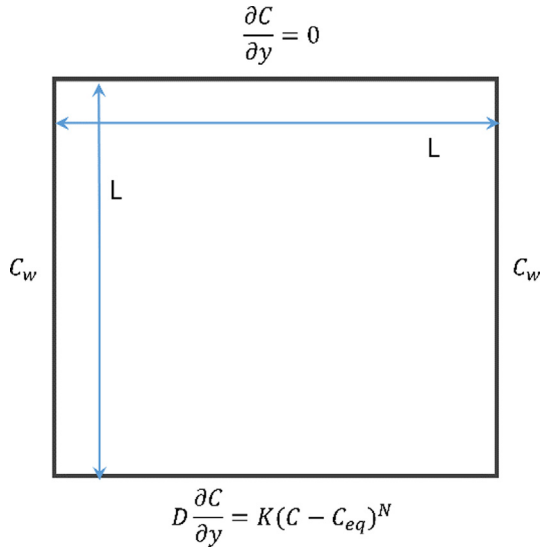

Fig. 9. Geometry and boundary conditions used for the problem of 2D diffusion.

be a linear Robin type and to reach a steady-state condition; they ignored volume alteration of the carbonate.

The physical parameters of the simulations and their corresponding lattice unit values are provided in Table 2. In this section, the newly proposed scheme was employed to impose the reaction boundary condition at the mineral's interface and for Dirichlet and Neumann concentration constraints at the inlet and outlet of the channel, the method of Zhang et al. (2012) was employed. Mesh independence was also checked but for brevity purposes the results are not presented.

The problem is simulated and the steady state concentration contour is shown in Fig. 12. As can be seen a small thickness concentration boundary layer is formed around the mineral, which is mainly because of the small value employed for diffusion coefficient.

To compare the results with those of Molins et al. (2020), pH values ($pH = -\log_{10}(\gamma C)$) along horizontal and vertical centerlines (x = 0.05, y = 0.025 cm) were also calculated and the results are illustrated in Fig. 13. As shown in this figure, a good agreement between the outcomes of this study and those of Molins et al. (2020) is observed.

4.2.4. Heterogeneous dissolution in a fracture

From an algorithmic point of view, the presented method offers two important characteristics; locality and orientation-independency. By locality, it is meant that the method requires no information of the neighboring sites to calculate the unknown populations of the current node. Also, orientation-independency

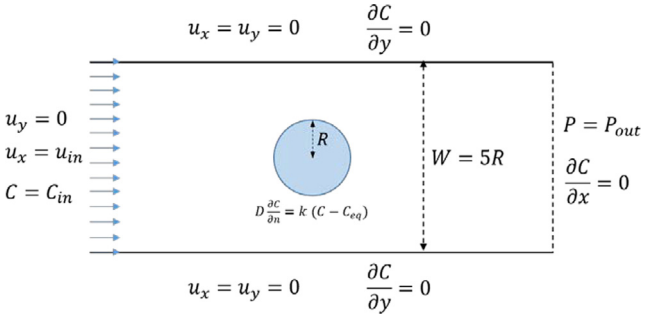

Fig. 11. Simulated geometry and the employed boundary conditions.

Table 2
Parameters of the simulations (physical and LBM values).

Parameter	Symbol	Physical value	LBM value
Wide of channel	w	0.05 cm	128
Length of channel	L	0.1 cm	256
Radius of grain	R	0.01 cm	25.6
Fluid density	ρ	1 gr cm^{-3}	1
Kinematic Viscosity ($\upsilon = c_s^2(\tau' - 0.5)$)	υ	10^{-2} cm^2s^{-1}	0.167
Diffusion Coefficient (Section 4.2.3)	D	10^{-5} cm^2s^{-1}	1.67×10^{-4}
Diffusion Coefficient (Section 4.2.5)	D	10^{-3} cm^2s^{-1}	1.67×10^{-2}
Inlet velocity	u	0.12 cm s^{-1}	7.8×10^{-4}
Inlet concentration	C	10^{-5} mol cm^{-3}	10^{-5}
Concentration at equilibrium	C_{eq}	0 mol cm^{-3}	0
Reaction Rate constant	k	$10^{-4.05}$ mol cm^{-2} s^{-1}	5.8×10^{-4}
Activity coefficient	γ	1000 cm^3 mol^{-1}	1
Reynolds number	$Re = \frac{uw}{\upsilon}$	0.6	0.6
Peclet number	$Pe = \frac{uw}{D}$	600	600
Damkohler number	$Da = \frac{K\gamma 2R}{D}$	178	178

means that the method is not restricted to flat boundaries and can easily and efficiently handle complex geometries with arbitrary orientation. However, the claimed orientation-independency of the scheme should not be confused with curvature recunstruction idea behind many conventional curved boundary treatment techniques. Here, by orientation-independency it is meant that to find the unknown distributions at fluid-solid interface, the position of the interface node and the number of unknown links in that node is not a restriction to the scheme; a feature, which is generally not garanteed in many other boundary schemes proposed so far (see for example the proposed boundary condition in (He et al., 1998), which is restricted to flat boundaries).

It should be emphasized that these two features -especially the latter one- would be essentially useful for efficient computation of transport phenomena in complex structures. Accordingly, the

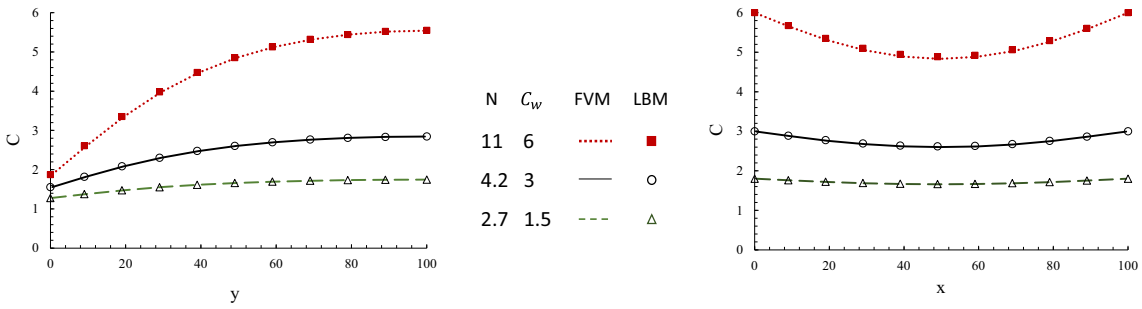

Fig. 10. Comparison of LBM and FVM results for different values of N and C_w on **(a)** vertical centerline and **(b)** Horizontal centerline.

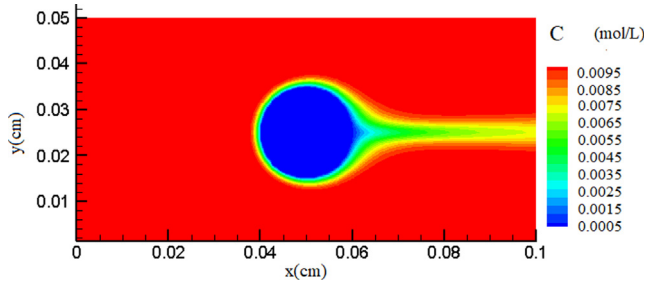

Fig. 12. Steady state concentration contours for the acid-carbonate reaction problem.

performance and accuracy of the method in geometry evolution problems are investigated by simulating a heterogeneous dissolution process in a simple fracture. Fig. 14 shows the geometry employed for this purpose. It should be pointed out that this problem has been previously studied in a number of researches and the interested reader is referred to (Kang et al., 2014; Taahodi et al., 2021) for more information.

The problem considers the flow of a solvent into a fracture of width H and aperture h. The solvent reacts with the horizontal interface of the fracture while the vertical boundaries are assumed insoluble. The governing macroscopic equations for this problem are given in Appendix A. The time evolution of the solid phase is calculated by:

$$\frac{\partial \forall}{\partial t} = \overline{V} a k (C_b - C_{eq})^N \tag{28}$$

where $\forall$is the solid volume fraction that evolves by time, $\overline{V}$ is the molar volume of mineral which is defined as 36.9 and a is the specific surface area of the solid phase which is assumed 1 for more simplicity (Kang et al., 2006). The other parameters are defined as $P_{in} = \frac{1}{3}$, $P_{out} = \frac{0.99}{3}$, $C_{eq} = 1, k = 0.0000267$, *and* $D = \frac{0.5}{3}$. At a low relative strength of reaction to diffusion (Damköhler number) and unreactive vertical walls, uniform dissolution of the lateral walls is expected (Kang et al., 2014; Taahodi et al., 2021). In this case, analytical analysis of the permeability porosity relationship for the medium leads to (Taahodi et al., 2021):

$$\frac{K_H}{K_H^0} = \left(\frac{h}{h_0}\right)^3 = \left(\frac{h/H}{h_0/H}\right)^3 = \left(\frac{\varepsilon}{\varepsilon_0}\right)^3 \tag{29}$$

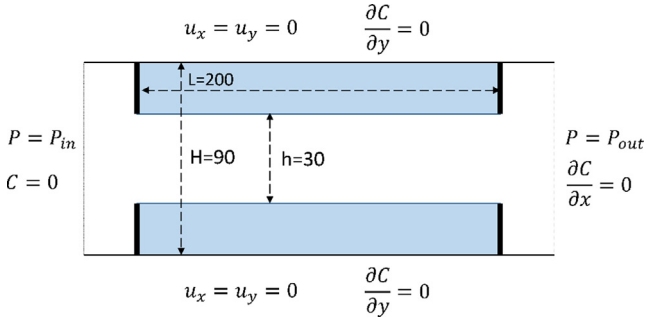

Fig. 14. Geometry of the medium used for fracture dissolution problem (the four vertical bold lines are assumed as insoluble boundaries).

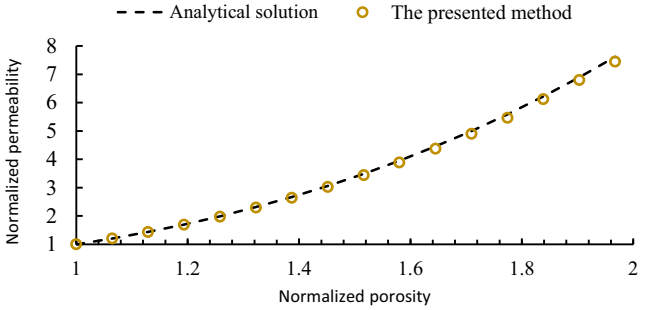

Fig. 15. Comparison of simulated normalized permeability and porosity relationship between the analytical solution and the presented method.

where h_0 is the initial fracture aperture, ε_0 is the initial porosity, K_H^0 is the initial permeability of the whole medium and the variables without 0 subscripts are the instantaneous ones during the dissolution progress. According to Eq. (29), a cubic polynomial is expected for the plot of normalized permeability versus normalized porosity. Simulation of the case with nonlinear reaction kinetics is performed and the result of the permeability-porosity relationship is illustrated in Fig. 15. As can be observed from the figure, the permeability evolution pattern of LBM agrees very well with that of the analytical solution.

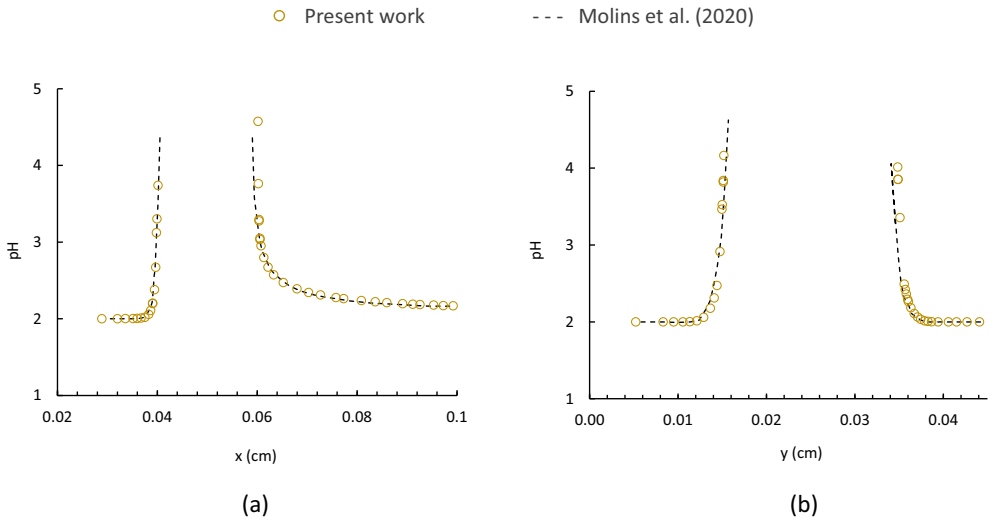

Fig. 13. pH values along (a) horizontal (b) vertical centerlines and their comparison with the results of Molins et al.(2020).

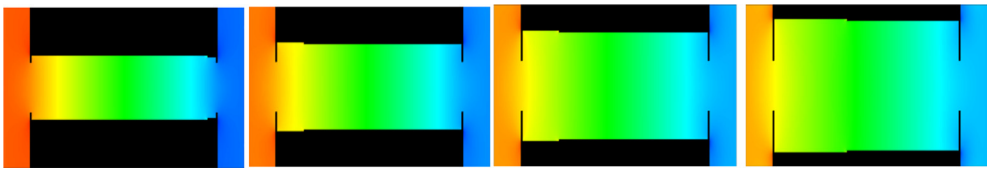

Fig. 16. Geometry evolution of the fracture at normalized porosities of 1.2, 1.6, 2.0, and 2.4 from left to right (colormap map indicating pressure contour).

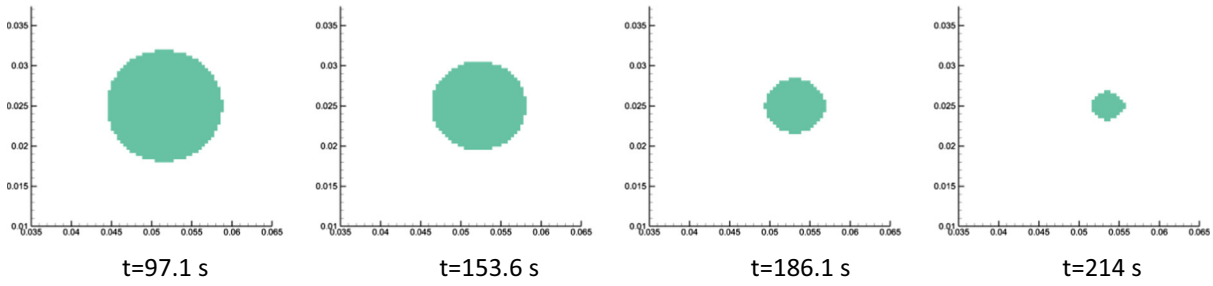

Fig. 17. Snapshots of geometry evolution with time at 4 different instantaneous volumes of the carbonate grain (V_0 representing the initial volume of the solid phase).

In addition, for more insight into the problem and to better see the desired uniform dissolution, the time evolution of the fracture geometry is shown in Fig. 16.

4.2.5. Heterogeneous dissolution of a carbonate grain

To consider a more complex system similar to those occurring in porous media, the problem of Section 4.2.3 was re-simulated but this time, the volume reduction and dynamic change of the geometry of the grain were also considered. The time evolution of the solid phase was calculated by Eq. (28) and the specific surface area of the solid phase (a) was calculated by the method of volume of fluid (Pilliod and Puckett, 2004). For the present case, the employed parameters were assumed the same as those in Table 2 but to speed up the dissolution process Peclet number was reduced to 6 to increase reaction rate (i.e. diffusion coefficient was increased for the simulations of this section). Since the grain surface was exposed to a reactive flow and because of the associated acid-carbonate dissolution, the grain size is expected to decrease over time. This phenomenon was confirmed in simulations and the results are shown in Fig. 17.

The time variation of the surface area of the grain was also calculated and the results were compared with those of Molins et al. (2020). As can be seen in Fig. 18, the outcomes of the present work are in a good agreement with those of Molins et al. (2020).

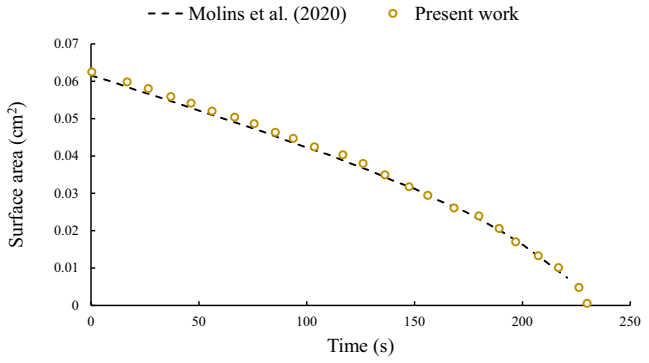

Fig. 18. Time variation in particle's surface area and the comparison with those of Molins et al. (2020).

5. Conclusions

Despite the applications in heat and mass transfer problems, the implementation of nth degree linear and nonlinear Robin boundary conditions in LBM framework have been a challenge so far. Accordingly, in this study, previously proposed counter-slip idea (Inamuro et al., 1995) and Taylor expansion method were employed and a novel general boundary scheme for the implementation of arbitrary nth order Robin boundary constraints was proposed.

The performance of the scheme was evaluated in a number of heat and mass transfer problems and the results were compared with analytical and numerical solutions. In case of unavailability of analytical solutions, finite volume solutions of the macroscopic equations were employed for comparison purposes.

For heat transfer test cases, surface convection (Newton's cooling law) and surface radiation problems were simulated. Comparison of the LBM results with available solutions demonstrated that the method performs very well in terms of accuracy. l^2-norm analysis of the scheme was also conducted and the results showed convergence rates of order between 1 and 2 for the method, varying with the constraint formulation and the exponent N.

For applications in mass transfer problems, a general boundary condition for n^{th}-order surface reactions was presented. The accuracy and convergence rate of the scheme were evaluated in a range of reaction orders and relaxation times. Analysis of the results indicated a good accuracy of the method.

From an algorithmic point of view, the presented method offers two important characteristics; locality and orientation-independency. Hence, it is believed that the method can be easily employed for simulation of coupled transport phenomena in complex geometries. To evaluate this characteristic, the problem of reactive flow in a simple fracture and time evolution of the solid nodes was investigated. To evaluate the performance of the proposed scheme in complex geometry, flow and transport around a grain with chemical reactions on its surface were investigated. Results of LBM for this test case indicated that the method can also be used in complex geometries with satisfying ease and accuracy.

CRediT authorship contribution statement

Elham Kashani: Investigation, Methodology, Writing - original draft, Software. **Ali Mohebbi:** Conceptualization, Supervision,

Writing - review & editing. **Amir Ehsan Feili Monfared:** Conceptualization, Supervision, Writing - review & editing. **Amir Raoof:** Conceptualization, Writing - review & editing.

Declaration of Competing Interest

The authors declare that they have no known competing financial interests or personal relationships that could have appeared to influence the work reported in this paper.

Acknowledgements

The authors would like to express their appreciation to the management of computer center of Chemical Engineering Department, Shahid Bahonar University of Kerman, Kerman, Iran, for supporting this work.

Appendix A: Governing equations

- The macroscopic boundary conditions in Section 4.2.2 are as follows:

$$C(x=0,y)=C_w \tag{A.1}$$

$$C(x=L,y)=C_w \tag{A.2}$$

$$\frac{\partial C}{\partial y}(x,y=L)=0 \tag{A.3}$$

$$D\frac{\partial C}{\partial y}(x,y=0)=K(C(x,y=0)-C_{eq})^N \tag{A.4}$$

- The macroscopic boundary conditions in Section 4.2.4 are as follow:

$$P(x=0,y,t)=P_{in} \tag{A.5}$$

$$P(x=L,y,t)=P_{out} \tag{A.6}$$

$$u(x,y=0,t)=0 \tag{A.7}$$

$$u(x,y=H,t)=0 \tag{A.8}$$

$$u(fluid-solid\ interface)=0 \tag{A.9}$$

and for the mass transfer part we have:

$$\mathrm{C(x,y,t=0)=C_{eq}} \tag{A.10}$$

$$\mathrm{C(x=0,y,t)=0} \tag{A.11}$$

$$\frac{\partial \mathrm{C}}{\partial \mathrm{y}}(\mathrm{x,y=0,t})=0 \tag{A.12}$$

$$\frac{\partial \mathrm{C}}{\partial \mathrm{y}}(\mathrm{x,y=H,t})=0 \tag{A.13}$$

$$\frac{\partial \mathrm{C}}{\partial \mathrm{x}}(\mathrm{x=L,y,t})=0 \tag{A.14}$$

and the reaction boundary condition at the fluid-solid interface on the horizontal face of the fracture is assumed to be of the form:

$$\mathrm{D}\frac{\partial \mathrm{C}}{\partial \mathrm{n}}=\mathrm{k(C-C_{eq})^N} \tag{A.15}$$

References

Ague, J.J., n.d. Fluid Flow in the Deep Crust, Treatise on Geochemistry, second ed. Elsevier Ltd., 203–247. https://doi.org/10.1016/B0-08-043751-6/03023-1.

Chai, Z., Zhao, T.S., 2013. Lattice Boltzmann model for the convection-diffusion equation. Phys. Rev. E – Stat. Nonlinear, Soft Matter Phys. 87, 1–15. https://doi.org/10.1103/PhysRevE.87.063309.

Chen, Q., Zhang, X., Zhang, J., 2013. Improved treatments for general boundary conditions in the lattice Boltzmann method for convection-diffusion and heat transfer processes. Phys. Rev. E – Stat. Nonlinear, Soft Matter Phys. 88. https://doi.org/10.1103/PhysRevE.88.033304.

D'Orazio, A., Corcione, M., Celata, G.P., 2004. Application to natural convection enclosed flows of a lattice Boltzmann BGK model coupled with a general purpose thermal boundary condition. Int. J. Therm. Sci. 43, 575–586. https://doi.org/10.1016/j.ijthermalsci.2003.11.002.

D'Orazio, A., Succi, S., 2003. Boundary Conditions for Thermal Lattice Boltzmann Simulations. Comput. Math. Appl., 977–986 https://doi.org/10.1007/3-540-44860-8_101.

Feili Monfared, A.E., Sarrafi, A., Jafari, S., Schaffie, M., 2016. Linear and non-linear Robin boundary conditions for thermal lattice Boltzmann method: Cases of convective and radiative heat transfer at interfaces. Int. J. Heat Mass Transf. 95, 927–935. https://doi.org/10.1016/j.ijheatmasstransfer.2015.12.055.

Ginzburg, I., 2005. Generic boundary conditions for lattice Boltzmann models and their application to advection and anisotropic dispersion equations. Adv. Water Resour. 28, 1196–1216. https://doi.org/10.1016/j.advwatres.2005.03.009.

Guo, Z., Zhao, T.S., 2002. Lattice Boltzmann model for incompressible flows through porous media. Phys. Rev. E - Stat. Physics, Plasmas, Fluids. Relat. Interdiscip. Top. 66, 1–9. https://doi.org/10.1103/PhysRevE.66.036304.

He, X., Chen, S., Doolen, G.D., 1998. A Novel Thermal Model for the Lattice Boltzmann Method in Incompressible Limit. J. Comput. Phys. 3146, 282–300.

He, X., Doolen, G.D., 2002. Thermodynamic foundations of kinetic theory and Lattice Boltzmann models for multiphase flows. J. Stat. Phys. 107, 309–328. https://doi.org/10.1023/A:1014527108336.

He, X., Li, N., Goldstein, B., 2000. Lattice Boltzmann simulation of diffusion-convection systems with surface chemical reaction. Mol. Simul. 25, 145–156. https://doi.org/10.1080/08927020008044120.

Huang, H.B., Lu, X.Y., Sukop, M.C., 2011. Numerical study of lattice Boltzmann methods for a convection-diffusion equation coupled with Navier-Stokes equations. J. Phys. A Math. Theor. 44. https://doi.org/10.1088/1751-8113/44/5/055001.

Huang, J., Yong, W., 2015. Boundary conditions of the lattice Boltzmann method for convection – diffusion equations. J. Comput. Phys. 300, 70–91. https://doi.org/10.1016/j.jcp.2015.07.045.

Huber, C., Shafei, B., Parmigiani, A., 2014. A new pore-scale model for linear and non-linear heterogeneous dissolution and precipitation. Geochim. Cosmochim. Acta 124, 109–130. https://doi.org/10.1016/j.gca.2013.09.003.

Inamuro, T., Yoshino, M., Ogino, F., 1995. A non-slip boundary condition for lattice Boltzmann simulations. Phys. Fluids 7, 2928–2930. https://doi.org/10.1063/1.868766.

Jeschke, A.A., Dreybrodt, W., 2002. Pitfalls in the determination of empirical dissolution rate equations of minerals from experimental data and a way out: An iterative procedure to find valid rate equations, applied to Ca-carbonates and -sulphates. Chem. Geol. 192, 183–194. https://doi.org/10.1016/S0009-2541(02)00135-3.

Ju, L., Zhang, C., Guo, Z., 2020. Local reactive boundary scheme for irregular geometries in lattice Boltzmann method. Int. J. Heat Mass Transf. 150,. https://doi.org/10.1016/j.ijheatmasstransfer.2020.119314 119314.

Kalia, N., Glasbergen, G., 2009. Wormhole formation in carbonates under varying temperature conditions. 8th Eur. Form. Damage Conf. 2009 - New Technol. Conv. Unconv. Reserv. 1, 386–404. https://doi.org/10.2118/121803-ms.

Kang, Q., Chen, L., Valocchi, A.J., Viswanathan, H.S., 2014. Pore-scale study of dissolution-induced changes in permeability and porosity of porous media. J. Hydrol. 517, 1049–1055. https://doi.org/10.1016/j.jhydrol.2014.06.045.

Kang, Q., Lichtner, P.C., Zhang, D., 2006. Lattice Boltzmann pore-scale model for multicomponent reactive transport in porous media. J. Geophys. Res. Solid Earth 111, 1–12. https://doi.org/10.1029/2005JB003951.

Kang, Q., Zhang, D., Chen, S., 2003. Simulation of dissolution and precipitation in porous media. J. Geophys. Res. Solid Earth 108, 1–10. https://doi.org/10.1029/2003jb002504.

Kang, Q., Zhang, D., Chen, S., He, X., 2002. Lattice Boltzmann simulation of chemical dissolution in porous media. Phys. Rev. E – Stat. Physics, Plasmas, Fluids, Relat. Interdiscip. Top. 65. https://doi.org/10.1103/PhysRevE.65.036318.

Karimipour, A., 2012. Simulation of Mixed Convection Heat Transfer in Macro and Microchannels by Using Lattice Boltzmann Method. University of Sistan & Baluchestan.

Keir, R.S., 1980. The dissolution kinetics of biogenic calcium carbonates in seawater. Geochim. Cosmochim. Acta 44, 241–252. https://doi.org/10.1016/0016-7037(80)90135-0.

Lasaga, A.C., 2014. Kinetic theory in the earth sciences. Chemistry. https://doi.org/10.5860/choice.36-4499.

Latt, J., Chopard, B., Malaspinas, O., Deville, M., Michler, A., 2008. Straight velocity boundaries in the lattice Boltzmann method. Phys. Rev. E 77,. https://doi.org/10.1103/PhysRevE.77.056703 056703.

Li, L., Mei, R., Klausner, J.F., 2013. Boundary conditions for thermal lattice Boltzmann equation method. J. Comput. Phys. 237, 366–395. https://doi.org/10.1016/j.jcp.2012.11.027.

Ma, X., Mou, J., Lin, H., Jiang, F., Liu, K., Zhao, X., 2017. Lattice Boltzmann Simulation of Wormhole Propagation in Carbonate Acidizing. J. Energy Resour. Technol. 139. https://doi.org/10.1115/1.4035909.

Mohamad, A.A., 2011. Lattice Boltzmann Method. Springer, London, London.

Molins, S., Soulaine, C., Prasianakis, N.I., Abbasi, A., Poncet, P., Ladd, A.J.C., Starchenko, V., Roman, S., Trebotich, D., Tchelepi, H.A., Steefel, C.I., 2020. Simulation of mineral dissolution at the pore scale with evolving fluid-solid interfaces: review of approaches and benchmark problem set. Comput. Geosci. https://doi.org/10.1007/s10596-019-09903-x.

Mostaghimi, P., Liu, M., Arns, C.H., 2016. Numerical Simulation of Reactive Transport on Micro-CT Images. Math. Geosci. 48, 963–983. https://doi.org/10.1007/s11004-016-9640-3.

Mozafari-shamsi, M., Sefid, M., Imani, G., 2018. PT US CR. Comput. Fluids. https://doi.org/10.1016/j.compfluid.2018.02.035.

Pilliod, J.E., Puckett, E.G., 2004. Second-order accurate volume-of-fluid algorithms for tracking material interfaces. J. Comput. Phys. 199, 465–502. https://doi.org/10.1016/j.jcp.2003.12.023.

Ponce Dawson, S., Chen, S., Doolen, G.D., 1993. Lattice Boltzmann computations for reaction-diffusion equations. J. Chem. Phys. 98, 1514–1523. https://doi.org/10.1063/1.464316.

Rudman, M., 1997. Volume-tracking methods for interfacial flow calculations. Int. J. Numer. Methods Fluids 24, 671–691. https://doi.org/10.1002/(SICI)1097-0363(19970415)24:7<671::AID-FLD508>3.0.CO;2-9.

Shan, X., Doolen, G., 1995. Multicomponent lattice-Boltzmann model with interparticle interaction. J. Stat. Phys. 81, 379–393. https://doi.org/10.1007/BF02179985.

Taahodi, M., Mohebbi, A., Feili Monfared, A.E., 2021. Lattice Boltzmann study of porosity-permeability variation in different regimes of non-isothermal dissolution in porous media. J. Pet. Sci Eng 202.

Tang, G.H., Tao, W.Q., He, Y.L., 2005. Thermal boundary condition for the thermal lattice Boltzmann equation 1–6. Phys. Rev. E. https://doi.org/10.1103/PhysRevE.72.016703.

Tian, Z., Xing, H., Tan, Y., Gao, J., 2014. A coupled lattice Boltzmann model for simulating reactive transport in CO2 injection. Phys. A Stat. Mech. Appl. 403, 155–164. https://doi.org/10.1016/j.physa.2014.02.040.

Walsh, S.D.C., Saar, M.O., 2010. Interpolated lattice Boltzmann boundary conditions for surface reaction kinetics. Phys. Rev. E – Stat. Nonlinear, Soft Matter Phys. 82, 1–10. https://doi.org/10.1103/PhysRevE.82.066703.

Yi, S., Wang, Q., Sun, W., 2014. An assessment of the role of nonlinear reaction kinetics in parameterization of metamorphic fluid flo. J. Geophys. Res. Solid Earth 119, 6249–6262. https://doi.org/10.1002/2015JB012608.Received.

Yoshino, M., Inamuro, T., 2003. Lattice Boltzmann simulations for flow and heat/mass transfer problems in a three-dimensional porous structure. Int. J. Numer. Methods Fluids 43, 183–198. https://doi.org/10.1002/fld.607.

Youngs, D.L., 1984. An interface tracking method for a 3D Eulerian Hydrodynamics code. Awre.

Zhang, T., Shi, B., Guo, Z., Chai, Z., Lu, J., 2012. General bounce-back scheme for concentration boundary condition in the lattice-Boltzmann method. Phys. Rev. E – Stat. Nonlinear, Soft Matter Phys. 85, 1–14. https://doi.org/10.1103/PhysRevE.85.016701.

Zou, Q., He, X., 1997. On pressure and velocity boundary conditions for the lattice Boltzmann BGK model. Phys. Fluids 9, 1591–1598. https://doi.org/10.1063/1.869307.